Journal of Materials Chemistry A

Accepted Manuscript

ROYAL SOCIETY OF CHEMISTRY

www.rsc.org/materialsA

Journal Name

ARTICLE

Synergistic Effect Between Layer Surface Configurations and K Ions of Potassium Vanadate Nanowires for Enhanced Energy Storage Performance

Received 00th January 20xx,
Accepted 00th January 20xx

DOI: 10.1039/x0xx00000x

www.rsc.org/

Jiashen Meng,† Ziang Liu,† Chaojiang Niu,† Xiaoming Xu, Xiong Liu, Guobin Zhang, Xuanpeng Wang, Meng Huang, Yang Yu, Liqiang Mai*

Layered metal vanadates, especially alkali metal vanadates have been extensively studied in energy storages. Generally, the vanadates exhibit more stable electrochemical performance than the pristine vanadium oxides, for another, different vanadates also vary in the performance. However, the detailed mechanisms of the variation in performance of vanadates and vanadium oxides are poorly explored. Here we choose and construct three typical layered vanadium-based nanowires (V_2O_5, KV_3O_8 and $K_{0.25}V_2O_5$), and investigate the origin of enhanced electrochemical performance of the potassium vanadates compared to V_2O_5, based on crystal structure analysis, electrochemical tests, *ex-situ* ICP measurements and *in-situ* XRD detections. We demonstrate a synergistic effect between layer surface configurations and K ions of potassium vanadate nanowires, which leads to the great improvement in electrochemical stability for $K_{0.25}V_2O_5$. The layer surface configuration of $K_{0.25}V_2O_5$ only consists of single-connected oxygen atoms, which provides strong interaction with the K ions. And the stabilized K ions act as "pillars" between interlayers to protect the layered structures from collapse in the charge/discharge process. This work provides a further insight of alkali metal vanadates, and benefits to the design of ideal electrode materials in energy storage field.

Introduction

With the rapid development of portable electronics, electric vehicles (EV) and hybrid electric vehicles (HEV), rechargeable batteries are undoubtedly one of the best candidates among various energy storage devices for chemically storing energy.[1] Till now, intensive efforts have been focused on developing rechargeable batteries with high energy density, high power density, high cycling stability and low cost.[2-5] Compared with anode materials, cathode materials become a big bottleneck of the battery breakthroughs due to their relatively low capacities.[6-9] Therefore, developing battery cathode materials with high capacity and low cost has been a crucial issue for both fundamental study and practical application.[10-14]

Generally, the cathode materials can be categorized into four main groups by their crystal structures: layer type, spinel type, olivine type, and NASICON type.[15-21] Among them, the layered oxides are one of the most extensively studied topics in lithium and sodium ion batteries. To our knowledge, well-developed and commercial layered oxides, such as $LiCoO_2$, $LiNi_{1/3}Co_{1/3}Mn_{1/3}O_2$ *etc.* have been widely investigated and applied for lithium-ion batteries.[16] Moreover, for sodium ion batteries, the common Na_xMeO_2 layered oxides (Me=3d transition metals), are built up of a sheet of edge-sharing [MeO_6] octahedra.[4] For example, Komaba *et al.* reported P2-$Na_{2/3}Fe_{1/2}Mn_{1/2}O_2$ made from earth-abundant elements, that delivers a reversible capacity of 190 mAh g^{-1} in sodium cells.[20] Therefore, intensive efforts have been dedicated to develop layered oxides with differernt stacked units in period, varying in their electrochemical performance for lithium and sodium ion batteries.[22-24]

Due to their abundant resources, easy preparation, stable thermodynamic properties and high theoretical capacities, vanadates, such as LiV_3O_8, $Na_{1.25}V_3O_8$, NaV_6O_{15}, $K_{0.25}V_2O_5$ *etc*, have been remarkably attractive candidates among layered oxides as lithium and sodium ion battery cathodes.[25-31] Liu *et al.* fabricated single crystalline NaV_6O_{15} nanorods via a hydrothermal route, which possessed enhanced electrochemical behaviour as a cathode in rechargeable lithium ion batteries.[26] Due to their structural stability and increased interlayer spaces, these vanadates also exhibit excellent sodium storage properties. Dong *et al.* reported hierarchical zigzag $Na_{1.25}V_3O_8$ nanowires, showing superior cycling stability and high rate capacities as a sodium ion battery cathode.[32] In our previous report, we investigated the isostructural alkali metal vanadates (Li, Na, K-V_6O_{15}) as lithium ion battery cathodes.[33] It is found that K-V_6O_{15} exhibits better electrochemical performance than V_2O_5, and also shows better rate capability and cycling stability than Li-V_6O_{15} and Na-V_6O_{15}. Based on experimental characterization

State Key Laboratory of Advanced Technology for Materials Synthesis and Processing, Wuhan University of Technology, Wuhan 430070, China
**E-mail: mlq518@whut.edu.cn*
† These authors are contributed equally to this work.
Electronic Supplementary Information (ESI) available: Crystallographic parameters,CV curves, AC impedance plots, XRD pattern and SEM image of $H_2V_3O_8$ nanowires, ICP test results. See DOI: 10.1039/x0xx00000x

and theoretical calculations, a synergistic effect between the layer surface structure and different alkali metal ions was proposed.[32]

To further demonstrate the synergistic effect and explore the enhanced mechanism in electrochemical performance, this work focuses on the vanadates with different layer surface configurations and the same alkaline metal ions. Here we purposefully choose and construct three typical layered vanadium-based nanowires (V_2O_5, KV_3O_8 and $K_{0.25}V_2O_5$), and investigate the origin of enhanced electrochemical performance of the potassium vanadates. The layer surface configurations of the potassium vanadates play a key role in their electrochemical stability. The K ions between interlayers in $K_{0.25}V_2O_5$ are more stable than those in KV_3O_8 due to the stronger interaction between K ions and single-connected oxygen atoms on the layer surface. And the stabilized K ions act as "pillars" between interlayers to protect the layered structures from collapse during the charge/discharge processes. Therefore, the synergistic effect between layer surface configurations and K ions is of great importance for the performance of potassium vanadate nanowires.

Experimental

Preparation of V_2O_5 nanowires

First, single crystalline $H_2V_3O_8$ nanowires were synthesized by a hydrothermal method according to our previous work.[33] Briefly, 1.3 mmol as-prepared V_2O_5 sol, 3.6 mL aniline, and 0.04 g poly(ethylene glycol) (PEG-4000) were mixed by stirring and then transferred into a telfon-lined stainless steel autoclave and kept at 180 ^{o}C for 48 h. The products were collected and washed repeatedly with deionized water and ethanol, and finally dried at 80 ^{o}C for 12 h in air to obtain $H_2V_3O_8$ nanowires. Second, after $H_2V_3O_8$ nanowires were sintered at 400 ^{o}C for 2h, V_2O_5 nanowires were obtained.

Preparation of KV_3O_8 nanowires

$H_2V_3O_8$ nanowires and KOH were mixed in alcohol and stirred for 6 h. Then after drying at 70 ^{o}C for 6 h, the mixture was annealed at 400 ^{o}C for 10 h to get a reddish brown powder. KV_3O_8 nanowires were obtained.

Preparation of $K_{0.25}V_2O_5$ nanowires

In a typical synthesis, 0.100 g of polyethyleneglycol (PEG-4000), 0.1818 g of V_2O_5 powder, and 0.35 mL of KOH (1 mol L^{-1}) were added in 30 mL of deionized water under vigorous magnetic stirring at room temperature for 2 h. Then, the mixture was transferred to a 50 mL autoclave and maintained in an oven at 180 ^{o}C for 48 h. The products were collected and washed repeatedly with deionized water and ethanol, and finally dried at 80 ^{o}C for 12 h in air. Then, the dried sample was annealed at 525 ^{o}C for 5 h in air to obtain $K_{0.25}V_2O_5$ nanowires.

Materials characterization

The crystallographic information of the final products was measured using a Bruker D8 Discover X-ray diffractometer equipped with a Cu Kα radiation source; the samples were scanned over the 2θ range from 10° to 60° at room temperature. SEM images were collected using a JEOL-7100F scanning electron microscope, and TEM images were collected using a JEM-2100F transmission electron microscope. Inductively coupled plasma (ICP) test was carried out using Optima4300DV.

Electrochemical characterization

The 2016 coin cells were assembled in a glovebox filled with pure argon. The cathode was composed of a ground mixture of 70% active material, 20% acetylene black and 10% poly(tetrafluoroethylene) (PTFE). After coating onto aluminum foil, the electrode film was uniformly cut into about 0.5-cm^2 (area) round slices, weighing a total of about 1.2 mg; the corresponding areal mass loading was 2.4 mg cm^{-2}. For lithium ion batteries, lithium foil was used as the anode and a solution of $LiPF_6$ (1 M) in EC/DEC (1:1 vol/vol) was used as the electrolyte. For sodium ion batteries, sodium discs were used as the anode and 1 M $NaClO_4$ in a mixture of ethylene carbon/dimethyl carbonate (1:1 w/w) with 2.0 wt% propylene carbonate (electrolyte additive) was used as the electrolyte. Galvanostatic charge/discharge measurements were performed using a multichannel battery testing system (LAND CT2001A). Cyclic voltammograms (CV) and electrochemical impedance spectra (EIS) were collected at room temperature using an Autolab potentiostat/galvanostat. For *in-situ* XRD measurement, the electrode was placed right behind an X-ray-transparent beryllium window which also acts as a current collector. The *in-situ* XRD signals were collected using the planar detector in a still mode during the discharge-charge process, and each pattern took 2 min to acquire.

Results and discussion

Morphology and structure characterization

First, the crystal structures of V_2O_5, KV_3O_8 and $K_{0.25}V_2O_5$ are illustrated (Fig. 1). V_2O_5 is the typical layered structure with the layer spacing of 4.36 Å. In comparison, KV_3O_8 and $K_{0.25}V_2O_5$ exhibit the different layered structures with K ions distributed in the interlayers (Table S1). And the layer spacing expands to 7.58 Å for KV_3O_8 and 7.42 Å for $K_{0.25}V_2O_5$, respectively. Notably, these two potassium vanadates have different layer surface configurations (as the yellow balls display in Fig. 1). The layer surface of KV_3O_8 is composed of single-connected and tri-connected oxygen atoms. However, all the oxygen atoms on the layer surface of $K_{0.25}V_2O_5$ are single-connected, which can bond and provide strong interaction with K ions.

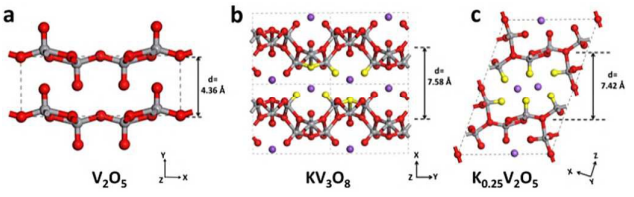

Fig. 1 Illustrations of the crystal structures of V_2O_5 (a), KV_3O_8 (b) and $K_{0.25}V_2O_5$ (c); respectively. The red and yellow balls represent O atoms; grey and purple balls represent V atoms and K ions, respectively.

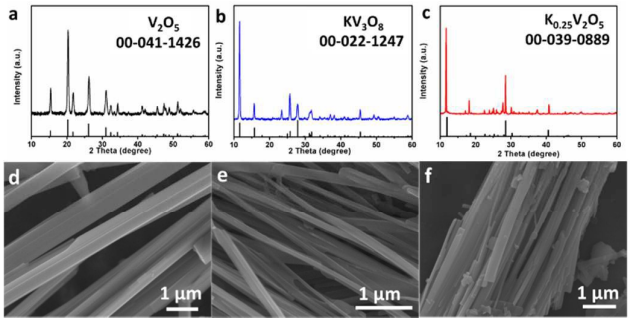

Fig. 2 XRD patterns and SEM images of V_2O_5 (a, d), KV_3O_8 (b, e) and $K_{0.25}V_2O_5$ (c, f) nanowires.

V_2O_5, KV_3O_8 and $K_{0.25}V_2O_5$ nanowires are synthesized via a facile hydrothermal method and subsequent heat treatment (Fig. S1).[34] Their XRD patterns show no impurities (Fig. 1a-c). V_2O_5 nanowires are orthorhombic phase (JCPDS No. 00-041-1426), while both KV_3O_8 and $K_{0.25}V_2O_5$ nanowires are both monoclinic phases (JCPDS No. 00-022-1247; JCPDS No. 00-039-0889). As the SEM images show, these nanowires display an average diameter of 100-300 nm and a smooth surface (Fig. 2d-f). As shown in TEM images, the length/diameter ratios are more than 50 (Fig. 3). From HRTEM images, the interlayer spacings of V_2O_5, KV_3O_8 and $K_{0.25}V_2O_5$ nanowires are calculated as 4.4 Å, 7.6 Å and 7.4 Å, consistent well with the corresponding lattice plane of (010), (100) and (002), respectively. These layers are in parallel to the nanowires.

Electrochemical performance

To compare the electrochemical performances of the V_2O_5, KV_3O_8 and $K_{0.25}V_2O_5$ nanowires, CV measurements are performed to explore the phase transformation at potentials ranging from 1.5 to 4.0 V and a scan rate of 0.2 mV s^{-1} (Fig. S2). As Fig. S2a shows, four sharp reduction peaks of V_2O_5 nanowires occur at potentials of 3.35, 3.14, 2.12, and 1.91 V, during the first discharge cycle. These sharp peaks correspond to the phase transformations from V_2O_5 to ε-$Li_{0.5}V_2O_5$, δ-LiV_2O_5, γ-$Li_2V_2O_5$ and ω-$Li_3V_2O_5$.[35-37] However, in the subsequent charge process, two broad oxidization peaks at 2.45

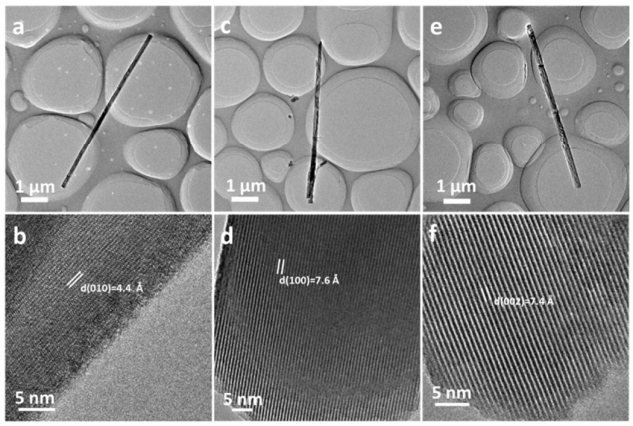

Fig. 3 TEM images of V_2O_5 (a, b), KV_3O_8 (c, d) and $K_{0.25}V_2O_5$ (e, f) nanowires, respectively.

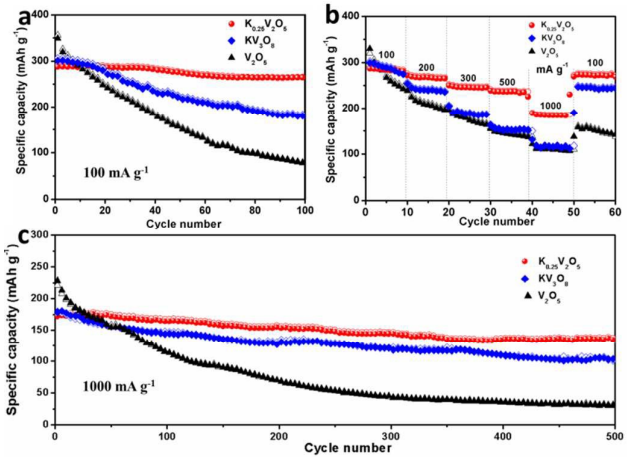

Fig. 4 Electrochemical performances of V_2O_5, KV_3O_8 and $K_{0.25}V_2O_5$ nanowires in lithium ion batteries. (a) Cycling performance tested at a low current density of 100 mA g^{-1}. (b) Rate performance tested at current densities of 100, 200, 300, 500 and 1000 mA g^{-1}. (c) Cycling performance tested at a high current density of 1000 mA g^{-1}.

and 2.68 V show obvious irreversible behaviour. The charge/discharge curves of V_2O_5 nanowires are characterized at a current density of 100 mA g^{-1} (Fig. S2d). After the first discharge process, the subsequent charge/discharge curves have no obvious voltage platforms, which are corresponding to broad peaks of CV curves. In previous report, the irreversible behaviour occurred in V_2O_5, which was due to the irreversible formation of ω-$Li_3V_2O_5$ at a voltage smaller than 1.9 V.[38] CV curve of KV_3O_8 nanowires have a pair of redox peaks, namely 2.33 V and 2.84 V (Fig. S2b). The corresponding charge-discharge curves of KV_3O_8 nanowires show that the first and second cycles are similar except for the small capacity fading (Fig. S2e). Compared with V_2O_5 and KV_3O_8 nanowires, $K_{0.25}V_2O_5$ nanowires exhibit better reversible behaviour and lower overpotential from CV and charge/discharge curves (Fig. S2c, f). Notably, the cathodic peaks below 1.9 V, corresponding to the irreversible phase transition of V_2O_5, disappeared in KV_3O_8 and $K_{0.25}V_2O_5$ nanowires.[38] To study the theoretical capacities of V_2O_5, KV_3O_8 and $K_{0.25}V_2O_5$ nanowires, the galvanostatic intermittent titration technique (GITT) test is conducted (Fig. S3). The V_2O_5 nanowires show a theoretical discharge capacity of 412 mAh g^{-1} (near 3 Li insertions per unit formula), which is consistent with those results previously reported.[36-38] The KV_3O_8 and $K_{0.25}V_2O_5$ nanowires show a theoretical discharge capacity of 327 and 341 mAh g^{-1}, respectively.

Meanwhile, more electrochemical measurements of V_2O_5, KV_3O_8 and $K_{0.25}V_2O_5$ nanowires were characterized for lithium ion batteries. When tested at a current density of 100 mA g^{-1}, the initial discharge capacities of V_2O_5, KV_3O_8 and $K_{0.25}V_2O_5$ nanowires are 353, 301, and 292 mAh g^{-1}, respectively. The initial discharge capacities of KV_3O_8 and $K_{0.25}V_2O_5$ nanowires are lower than that of V_2O_5 nanowires due to the partial occupation of K ions in available Li ion intercalation sites. The corresponding first coulombic efficiencies of V_2O_5, KV_3O_8 and $K_{0.25}V_2O_5$ nanowires in lithium ion batteries are 93%, 95%, and nearly 100%, respectively. Moreover, 20%, 55% and

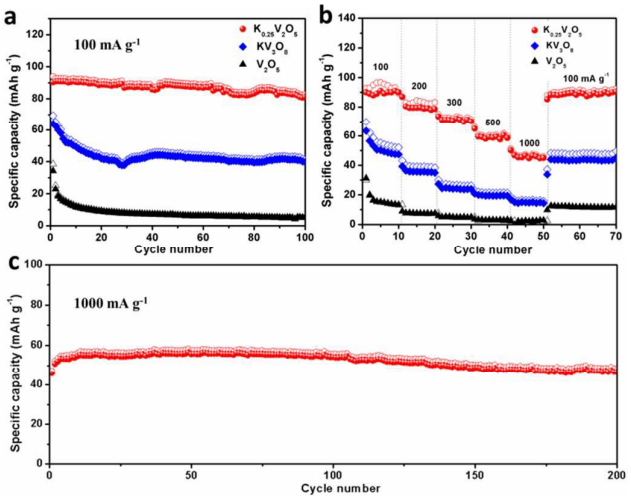

Fig. 5 Electrochemical performance of V_2O_5, KV_3O_8 and $K_{0.25}V_2O_5$ nanowires in sodium ion batteries. (a) Cycling performance tested at a low current density of 100 mA g^{-1}. (b) Rate performance tested at current densities of 100, 200, 300, 500 and 1000 mA g^{-1}. (c) Cycling performance of $K_{0.25}V_2O_5$ nanowires tested at a high current density of 1000 mA g^{-1}.

92% (i.e., 71, 165 and 270 mAh g^{-1}) were retained after 100 cycles at 100 mA g^{-1} (Fig. 4a). The rate performance was measured at various current densities of 100, 200, 300, 500, and 1000 mA g^{-1} (Fig. 4b). As Fig. 4b shows, the $K_{0.25}V_2O_5$ nanowires possess excellent rate performance. Average discharge capacities of 286, 273, 252, 241, and 187 mAh g^{-1}, respectively, were obtained at these rates. The corresponding charge/discharge curves at different current densities were shown in Fig. S4. When the current density was back to 100 mA g^{-1}, the average discharge capacity was 271 mAh g^{-1} with capacity recovery of 95%, superior to that of V_2O_5 and KV_3O_8 nanowires (i.e., 55% and 80%, respectively). In addition, when tested at a high current density of 1000 mA g^{-1}, the first discharge capacities of V_2O_5, KV_3O_8 and $K_{0.25}V_2O_5$ nanowires were 225, 178 and 172 mAh g^{-1}, with the capacity retention of 14%, 62% and 83% after 500 cycles, respectively (Fig. 4c). EIS measurements were carried out (Fig. S5). The charge transfer resistance (R_{ct}) of $K_{0.25}V_2O_5$ nanowires is 124 Ω, which is lower than those of V_2O_5 and KV_3O_8 nanowires (252 Ω and 170 Ω, respectively), showing higher efficient electron/ion transport. All results demonstrate that potassium vanadate nanowires exhibit better electrochemical performance than V_2O_5 when used as lithium ion battery cathodes. Meanwhile, $K_{0.25}V_2O_5$ nanowires show better electrochemical stability than the KV_3O_8 nanowires.

To further confirm the observed law above, V_2O_5, KV_3O_8 and $K_{0.25}V_2O_5$ nanowires were also characterized for sodium ion batteries. Initially, V_2O_5, KV_3O_8 and $K_{0.25}V_2O_5$ nanowires were tested at a current density of 100 mA g^{-1} (Fig. 5a). The first discharge capacities were 35, 68 and 90 mAh g^{-1}. After 100 cycles, the capacity retentions were 24%, 59% and 90%, respectively. The corresponding typical charge-discharge profiles of V_2O_5, KV_3O_8 and $K_{0.25}V_2O_5$ nanowires were shown in Fig. S6. As previously reported, orthorhombic V_2O_5 for sodium ion battery application experienced deterioration and eventual loss of crystallinity after cycling, leading

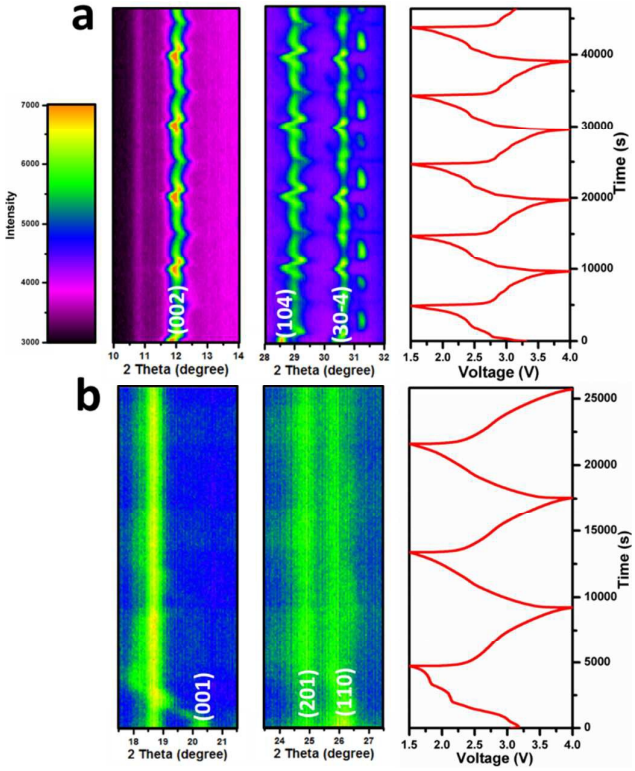

Fig. 6 *In-situ* X-ray diffraction patterns of $K_{0.25}V_2O_5$ nanowires (a) and V_2O_5 nanowires (b) during galvanostatic charge and discharge at 150 mA g^{-1} in lithium ion batteries. The horizontal axis represents the selected 2θ regions, and time is on the vertical axis. The diffraction intensity is colour coded with the scale bar shown on left. The corresponding voltage curve is plotted to the right.

to fast capacity fading.[39] Subsequently, the rate performance was determined at rates of 100, 200, 300, 500, and 1000 mA g^{-1} (Fig. 5b). When the current density was returned to 100 mA g^{-1}, the capacity recovery of $K_{0.25}V_2O_5$ nanowires was nearly 100% and the 70th-cycle discharge capacity reached to 90 mAh g^{-1}, showing great structural stability and excellent reversibility. Especially, a 88% retention of the top discharge capacity after 200 cycles at a high current density of 1000 mA g^{-1}, also testified the excellent cycling performance of $K_{0.25}V_2O_5$ nanowires (Fig. 5c).

Synergistic effect in potassium vanadate nanowires

To reveal the enhanced mechanism in electrochemical performance of potassium vanadate, $K_{0.25}V_2O_5$ and V_2O_5 nanowires were characterized by time-resolved *in-situ* XRD during lithium ion insertion and extraction. The clear variation of appropriate selective regions of $K_{0.25}V_2O_5$ and V_2O_5 nanowires was observed during the original cycles of galvanostatic charge and discharge at potentials ranging from 1.5 to 4.0 V and a current density of 150 mA g^{-1} (Fig. 6 and). In Fig. 6a, the (002), (104) and (30-4) reflection peaks of $K_{0.25}V_2O_5$ nanowires shift repeatedly during the galvanostatic charge and discharge process. Generally speaking, the lithium/sodium ions insert into the cathodes during the discharge process, and increase the interlayer spacings along with main peaks shifting toward low angles. Particularly, when the lithium ions insert into the $K_{0.25}V_2O_5$,

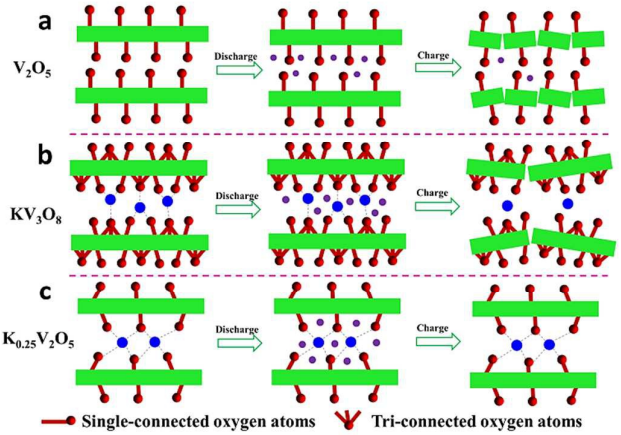

Fig. 7 Schematic illustrations of lithium/sodium intercalation/deintercalation processes of V_2O_5 (a), KV_3O_8 (b) and $K_{0.25}V_2O_5$ (c) for the initial cycles, respectively. The red balls, purple balls, and blue balls represent the O atoms, Li/Na ions and K ions, respectively.

these peaks shift toward to high angles. The lithium ion insertion process can be expressed as:

$$K_{0.25}V_2O_5 + xLi^+ + xe^- \rightarrow Li_xK_{0.25}V_2O_5.$$ [26]

The interlayer spacing of (002) changes from 7.42 Å to 7.14 Å based on Bragg equation. The crystal structure of $K_{0.25}V_2O_5$ consists of VO_5 pyramids and VO_6 octahedra to form the $(V_2O_5)_x$ frameworks. The lithium ion insertion may form the covalent bond with the oxygen among the $(V_2O_5)_x$ frameworks and reduce the average $(V_2O_5)_x$ anion radius. The changing amplitudes of main peaks are smaller than that of V_2O_5 nanowires. It indicates that K ions can act as "pillars" in between V-O layers to keep structural stability, increase parallel spacing and avoid the irreversible reaction. On the other hand, the selective (001), (201) and (110) reflection peaks of V_2O_5 nanowires change during the galvanostatic charge and discharge processes (Fig. 6b). It is obvious that the main diffraction peak of (001) disappears after the first discharge process, showing its irreversibility. At first, the length of the c-axis in V_2O_5 crystal cell increases at the shallow discharge process and then the structural integrity is destroyed at the deep discharge process. Combined with CV curves, the phases evolve from V_2O_5 to ε-$Li_{0.5}V_2O_5$, δ-LiV_2O_5, γ-$Li_2V_2O_5$ and ω-$Li_3V_2O_5$. As previously reported, the irreversible ω-$Li_3V_2O_5$ was formed and followed by wide solid solution process.[38]

To reveal the reason why $K_{0.25}V_2O_5$ nanowires show better electrochemical stability than KV_3O_8 nanowires, time-resolved *in situ* XRD results were first compared. In Fig. S7, the (100) reflection of KV_3O_8 nanowires shifts repeatedly for the initial charge and discharge process. However, compared with stable peaks of $K_{0.25}V_2O_5$, the (100) peak position of KV_3O_8 in the charge state shifts to high angle gradually after several cycles, and the peak become wider and intensity also decreases, which indicates the collapse and amorphization of the KV_3O_8 layered structure in the lithium insertion-extraction process. In addition, ICP test was carried out to directly detect the change of K ion amount in potassium vanadate nanowire cathodes. After 100 cycles at 100 mA g^{-1}, the coin cells were disassembled and the $K_{0.25}V_2O_5$ and KV_3O_8 nanowire cathodes were washed with pure alcohol and deionized water. The molar ratios of K:V in $K_{0.25}V_2O_5$ nanowire cathodes change from 0.252:2 to 0.241:2, corresponding to the K loss ratio of 4.4%. However, in KV_3O_8 nanowires, the molar ratios change from 1.013:3 to 0.792:3, and the K loss ratio is 21.8% (Table S2), indicating that the K ions in $K_{0.25}V_2O_5$ are more stable than in KV_3O_8. Therefore, the more stabilized K ions in the interlayers lead to better electrochemical stability.

On the basis of the crystal structure analysis, electrochemical tests, *in-situ* XRD detections and *ex-situ* ICP measurements, the lithium/sodium intercalation/deintercalation processes of V_2O_5, KV_3O_8 and $K_{0.25}V_2O_5$ can be illustrated as in Fig. 7.[40] For pristine V_2O_5 nanowires (Fig. 7a), owing to the lack of ion pillars, the intercalation of lithium/sodium ions into the interlayer sites will lead to an irreversible structure transformation and severe structure degradation in the initial cycles, and thus resulting in fast capacity loss. For potassium vanadate nanowires, the K ions between interlayers can bond with the single-connected oxygen atoms and act as "pillars" to protect the layered structures from collapse. However, for KV_3O_8, there are tri-connected oxygen atoms existing on the layer surface, which cannot provide strong interaction with the K ions, causing the instability of K ions in the interlayers. After several charge-discharge cycles, partial K ions extract from the crystal structure (as demonstrated by the ICP measurements) and thus leads to the weakening of the pillar effect. And then the structure degradation occurs (as demonstrated by the *in-situ* XRD results), which results in the capacity fading. For $K_{0.25}V_2O_5$ nanowires (Fig. 7c), the layer surface consists of only single-connected oxygen atoms, which can form strong interaction with K ions, and the firmly fixed K ions in the interlayers act as "pillars" to keep structural integrity and results in excellent cycling performance during the charge/discharge process.

In brief, the superior electrochemical stability of $K_{0.25}V_2O_5$ is attributed to the synergistic effect between its layer surface configuration and the K ions in the interlayers: the layer surface consisted of single-connected oxygen atoms provides strong interaction with the K ions, and the stable K ions in the interlayers act as "pillars" to prevent the structure from degradation, leading to outstanding electrochemical performance.

Conclusions

We purposefully prepared V_2O_5, KV_3O_8 and $K_{0.25}V_2O_5$ nanowires via a facile hydrothermal method and subsequent heat treatment. Compared with pristine V_2O_5, the potassium vanadate nanowires exhibit great improvement in electrochemical performance. Moreover, $K_{0.25}V_2O_5$ nanowires display better electrochemical stability than KV_3O_8 nanowires. Based on the crystal structure analysis, electrochemical tests, *in-situ* XRD detections and *ex-situ* ICP measurements, we conclude that the synergistic effect between layer surface configuration and the K ions results in the outstanding electrochemical stability of $K_{0.25}V_2O_5$ nanowire. Namely, the single-connected oxygen atoms on the layer surface provide strong interaction with the K ions, and the stable K ions in the interlayers act as "pillars" to prevent structure from degradation, leading to better electrochemical performance. This work provides a further

insight of the structure-property correlation of alkali metal vanadates when used as energy storage materials, and provides a better direction for the design of ideal electrode materials in energy storage field.

Acknowledgements

This work was supported by the National Basic Research Program of China (2013CB934103, 2012CB933003), the International Science & Technology Cooperation Program of China (2013DFA50840), the National Natural Science Foundation of China (51521001, 51272197), the National Natural Science Fund for Distinguished Young Scholars (51425204), the Hubei Provincial Natural Science Fund for Distinguished Young Scholars (2014CFA035), and the Fundamental Research Funds for the Central Universities (WUT: 2015-III-021, 2015-III-032, 2015-PY-2). We thank Prof. D. Y. Zhao of Fudan University and Prof. J. Liu of Pacific Northwest National Laboratory for useful discussions and assistance with the manuscript.

Notes and References

1 Z. G. Yang, J. L. Zhang, M. C. Kintner-Meyer, X. C. Lu, D. Choi, J. P. Lemmon and J. Liu, *Chem. Rev.*, 2011, **111**, 3577-3613.
2 M. Armand and J.-M. Tarascon, *Nature*, 2008, **451**, 652-657.
3 L. Q. Mai, X. C. Tian, X. Xu, L. Chang and L. Xu, *Chem. Rev.*, 2014, **114**, 11828-11862.
4 N. Yabuuchi, K. Kubota, M. Dahbi and S. Komaba, *Chem. Rev.*, 2014, **114**, 11636-11682.
5 V. Palomares, M. Casas-Cabanas, E. Castillo-Martínez, M. H. Han and T. Rojo, *Energy Environ. Sci.*, 2013, **6**, 2312-2337.
6 W. Luo, S. Lorger, B. Wang, C. Bommier and X. L. Ji, *Chem. Commun.*, 2014, **50**, 5435-5437.
7 Z. Y. Wang, L. Zhou and X. W. David Lou, *Adv. Mater.*, 2012, **24**, 1903-1911.
8 C. Yuan, H. B. Wu, Y. Xie and X. W. Lou, *Angew. Chem. Int. Ed.*, 2014, **53**, 1488-1504.
9 D. R. Rolison, J. W. Long, J. C. Lytle, A. E. Fischer, C. P. Rhodes, T. M. McEvoy, M. E. Bourg and A. M. Lubers, *Chem. Soc. Rev.*, 2009, **38**, 226-252.
10 F. Y. Cheng, J. Liang, Z. L. Tao and J. Chen, *Adv. Mater.*, 2011, **23**, 1695-1715.
11 C. J. Niu, J. S. Meng, X. P. Wang, C. H. Han, M. Y. Yan, K. N. Zhao, X. M. Xu, W. H. Ren, Y. L. Zhao, L. Xu, Q. J. Zhang, D. Y. Zhao and L. Q. Mai, *Nat. Commun.*, 2015, **6**, 7402.
12 Y. Zhao and L. Jiang, *Adv. Mater.*, 2009, **21**, 3621-3638.
13 G. Z. Fang, J. Zhou, Y. Hu, X. X. Gao, Y. Tang and S. Q. Liang, *J. Power Sources*, 2015, **275**, 694-701.
14 Q. Y. An, P. F. Zhang, Q. L. Wei, L. He, F. Y. Xiong, J. Z. Sheng, Q. Q. Wang and L. Q. Mai, *J. Mater. Chem. A*, 2014, **2**, 3297.
15 Y. H. Wang, Y. H. Wang, D. S. Jia, Z. Peng, Y. Y. Xia and G. F. Zheng, *Nano Lett.*, 2014, **14**, 1080-1084.
16 S. Luo, K. Wang, J. P. Wang, K. L. Jiang, Q. Q. Li and S. S. Fan, *Adv. Mater.*, 2012, **24**, 2294-2298.
17 C. B. Zhu, Y. Yu, L. Gu, K. Weichert and J. Maier, *Angew. Chem. Int. Ed.*, 2011, **50**, 6278-6282.
18 W. C. Duan, Z. Q. Zhu, H. Li, Z. Hu, K. Zhang, F. Y. Cheng and J. Chen, *J. Mater. Chem. A*, 2014, **2**, 8668.
19 X. P. Wang, C. J. Niu, J. S. Meng, P. Hu, X. M. Xu, X. J. Wei, L. Zhou, K. N. Zhao, W. Luo, M. Y. Yan and L. Q. Mai, *Adv. Energy Mater.*, 2015, **5**, 1500716.
20 N. Yabuuchi, M. Kajiyama, J. Iwatate, H. Nishikawa, S. Hitomi, R. Okuyama, R. Usui, Y. Yamada and S. Komaba, *Nat. Mater.*, 2012, **11**, 512-517.
21 X. H. Rui, W. P. Sun, C. Wu, Y. Yu and Q. Y. Yan, *Adv. Mater.*, 2015, **27**, 6670-6676.
22 G. Singh, J. M. L. del Amo, M. Galceran, S. Pérez-Villar and T. Rojo, *J. Mater. Chem. A*, 2015, **3**, 6954-6961.
23 Y. N. Zhou, J. Ma, E. Hu, X. Yu, L. Gu, K. W. Nam, L. Chen, Z. Wang and X. Q. Yang, *Nat. Commun.*, 2014, **5**, 5381.
24 J. Lee, A. Urban, X. Li, D. Su, G. Hautier and G. Ceder, *Science*, 2014, **343**, 519-522.
25 R. Baddour-Hadjean, A. Boudaoud, S. Bach, N. Emery and J. P. Pereira-Ramos, *Inorg. Chem.*, 2014, **53**, 1764-1772.
26 H. M. Liu, Y. G. Wang, L. Li, K. X. Wang, E. Hosono and H. S. Zhou, *J. Mater. Chem.*, 2009, **19**, 7885-7891.
27 S. Bach, A. Boudaoud, N. Emery, R. Baddour-Hadjean and J. P. Pereira-Ramos, *Electrochim. Acta*, 2014, **119**, 38-42.
28 W. Hu, X. B. Zhang, Y. L. Cheng, Y. M. Wu and L. M. Wang, *Chem. Commun.*, 2011, **47**, 5250-5252.
29 S. Yuan, Y. B. Liu, D. Xu, D. L. Ma, S. Wang, X. H. Yang, Z. Y. Cao and X. B. Zhang, *Adv. Sci.*, 2015, **2**, 1400018.
30 E. Uchaker and G. Z. Cao, *Chem Asian J*, 2015, **10**, 1608-1617.
31 W. Hu, X. B. Zhang, Y. L. Cheng, C. Y. Wu, F. Cao and L. M. Wang, *ChemSusChem*, 2011, **4**, 1091-1094.
32 Y. F. Dong, S. Li, K. N. Zhao, C. H. Han, W. Chen, B. L. Wang, L. Wang, B. A. Xu, Q. L. Wei, L. Zhang, X. Xu and L. Q. Mai, *Energy Environ. Sci.*, 2015, **8**, 1267-1275.
33 Y. L. Zhao, C. H. Han, J. W. Yang, J. Su, X. M. Xu, S. Li, L. Xu, R. P. Fang, H. Jiang, X. D. Zou, B. Song, L. Q. Mai and Q. J. Zhang, *Nano Lett.*, 2015, **15**, 2180-2185.
34 Q. Y. An, J. Z. Sheng, X. Xu, Q. L. Wei, Y. Q. Zhu, C. H. Han, C. J. Niu and L. Q. Mai, *New J. Chem.*, 2014, **38**, 2075-2080.
35 Y. L. Cheah, N. Gupta, S. S. Pramana, V. Aravindan, G. Wee and M. Srinivasan, *J. Power Sources*, 2011, **196**, 6465-6472.
36 Z. L. Wang, D. Xu, L. M. Wang and X. B. Zhang, *ChemPlusChem*, 2012, **77**, 124-128.
37 H. G. Wang, D. L. Ma, Y. Huang and X. B. Zhang, *Chem. Eur. J.*, 2012, **18**, 8987-8993.
38 L. Q. Mai, L. Xu, C. H. Han, X. Xu, Y. Z. Luo, S. Y. Zhao and Y. L. Zhao, *Nano Lett.*, 2010, **10**, 4750-4755.
39 D. W. Su and G. X. Wang, *ACS nano*, 2013, **7**, 11218-11226.
40 Y. F. Dong, X. M. Xu, S. Li, C. H. Han, K. N. Zhao, L. Zhang, C. J. Niu, Z. Huang and L. Q. Mai, *Nano Energy*, 2015, **15**, 145-152.

Here we design and construct three typical layered vanadium-based nanowires (V_2O_5, KV_3O_8 and $K_{0.25}V_2O_5$), and investigate the origin of enhanced electrochemical performance of the potassium vanadates.